

**V.I. Il'icev Pacific Oceanological Institute  
Far East Branch, Academy of Sciences of Russia  
Vladivostok, Russian Federation**

**'Approved'**  
POI FEB RAS Director  
Academic V.A. Akulichev  
March 2005

**Acoustic Studies on the North East Sakhalin Shelf  
Volume 2: Analysis, Conclusions and Recommendations**

**30 July to 7 October, 2004  
Sakhalin, Russian Federation**

**A.A. Karnauhov  
M.V. Kruglov  
A.N. Rutenko**

**Prepared for:  
Exxon Neftegas Limited  
&  
Sakhalin Energy Investment Company,**

**Yuzhno-Sakhalinsk, Sakhalin,  
Russian Federation**

**June, 2005**

## Table of Contents

<b>LIST OF TABLES .....</b>	<b>III</b>
<b>LIST OF FIGURES.....</b>	<b>III</b>
<b>EXECUTIVE SUMMARY .....</b>	<b>VIII</b>
<b>1 INTRODUCTION.....</b>	<b>1</b>
1.1 Acoustic recording and processing equipment	2
1.2 Low Frequency and High Frequency transducers and hydrological sonde	5
1.3 Terminology and algorithms used in the report	8
1.4 Units	8
<b>2 IMPACT OF WEATHER CONDITIONS ON THE AMBIENT ACOUSTIC FIELD OF THE NE SAKHALIN SHELF .....</b>	<b>9</b>
<b>3 ANALYSIS OF TRANSMISSION LOSS TL(F,R) EXPERIMENTS CONDUCTED ON THE SAKHALIN SHELF .....</b>	<b>20</b>
3.1 Discussion of the factors controlling TL(f,r) in shallow water	20
3.2 Analysis of propagation and TL from the pipeline routes to the Piltun feeding area	22
3.3 Analysis of TL from the Chayvo Pipeline to the Piltun and Offshore Feeding Areas	23
3.4 Analysis of TL from Orlan Platform to the Piltun and Offshore Feeding Areas	36
3.5 Analysis of TL from the Odoptu License to the Piltun Feeding Area	44
3.5 Analysis of TL from the Odoptu License to the Piltun Feeding Area	45
3.5 Analysis of TL from the Odoptu License to the Piltun Feeding Area	46
<b>4 ANALYSIS OF ACOUSTIC PULSES FROM MARINE LIFE, ANTHROPOGENIC AND NATURAL SEISMICITY .....</b>	<b>49</b>
4.1 Anthropogenic Impulses	49
4.2 Impulses of possible biogenic origin recorded in 2004	49
<b>5 ESTIMATION OF EXPOSURE LEVEL (EL) AT THE BEHAVIORAL OBSERVATION STATIONS.....</b>	<b>55</b>
<b>5 ESTIMATION OF EXPOSURE LEVEL (EL) AT THE BEHAVIORAL OBSERVATION STATIONS.....</b>	<b>56</b>
<b>5 ESTIMATION OF EXPOSURE LEVEL (EL) AT THE BEHAVIORAL OBSERVATION STATIONS.....</b>	<b>57</b>
5.1 Estimating energy levels at the acoustic monitor stations	57
<b>6 ACOUSTIC SIGNATURES OF THE <i>ACADEMIK OPARIN</i> AND PHOTO-ID ZODIACS..</b>	<b>62</b>
6.1 Acoustic measurements of the research vessel <i>Academik Oparin</i>	62
6.1.1 Acoustic measurements from the Igor Maksimov .....	62
6.1.2 Acoustic measurements on the Akademik Oparin in the Offshore feeding area .....	64

6.1.3 Acoustic measurements on the Akademik Oparin in the Piltun feeding area.....	67
6.2 Acoustic measurements of the Photo-ID zodiacs	70
6.2 Acoustic measurements of the Photo-ID zodiacs	71
<b>7 BATHYMETRIC AND HYDROLOGIC STUDIES ON THE NE SAKHALIN SHELF .....</b>	<b>76</b>
<b>7 BATHYMETRIC AND HYDROLOGIC STUDIES ON THE NE SAKHALIN SHELF .....</b>	<b>77</b>
<b>7 BATHYMETRIC AND HYDROLOGIC STUDIES ON THE NE SAKHALIN SHELF .....</b>	<b>78</b>
7.1 Bathymetry map	78
7.2 Impact of wind and tides on the thermohaline structure in August and September	78
7.2.1 Average values for August.....	86
7.2.1 Average values for August.....	87
7.2.2 Average values for September .....	87
<b>8 RESULTS AND CONCLUSIONS .....</b>	<b>91</b>
<b>9 FUTURE PLANS.....</b>	<b>97</b>
<b>10 ACKNOWLEDGEMENTS.....</b>	<b>99</b>
<b>10 ACKNOWLEDGEMENTS.....</b>	<b>100</b>
<b>11 AUTHORS .....</b>	<b>100</b>
<b>12 BIBLIOGRAPHY .....</b>	<b>101</b>
<b>APPENDIX A - DESCRIPTION OF DATA USED FOR THE TL STUDIES .....</b>	<b>105</b>

## LIST OF TABLES

Table 1.1. Numbers, names, locations and depths of the proposed stations.

Table 5.1. Relationship between the behavioral and acoustic monitoring stations.

## LIST OF FIGURES

Figure 1.1. 2003 and 2004 AUARs being prepared for deployment.

Figure 1.2. Map showing the AUAR locations and probability contours showing the density distributions of western gray whales from the 2002 to 2003 aerial surveys.

Figure 2.1. Sonogram  $G(f,t)$  and plot of the variation in sound pressure level with time  $D(\Delta f,t)$  over four frequency ranges for data recorded at location A.5 during a typhoon.

Figure 2.2. Spectra  $G(f)$  of noise synchronously (or close to synchronously) recorded at (a) acoustic station A.5 and (b) monitor station Arkutun-Dagi during a typhoon.

Figure 2.3. Sonogram  $G(f,t)$  and plot of the variation in sound pressure level with time  $D(\Delta f,t)$  for data recorded at monitor station Arkutun-Dagi from 19 to 31 August, 2004.

Figure 2.4. (a) Sonogram  $G(f,t)$  showing development of a storm on 24 August; (b) spectra  $G(f)$  of acoustic noise recorded at different phases of the storm - Arkutun-Dagi monitor station.

Figure 2.5. Sonogram  $G(f,t)$  and plot of the variation in sound pressure level with time  $D(\Delta f,t)$  for data recorded at monitor station Arkutun-Dagi from 7 to 19 September, 2004.

Figure 2.6. Sonogram  $G(f,t)$  and plot of the variation in sound pressure level with time  $D(\Delta f,t)$  for data recorded at monitor station Odoptu-S-10 from 10 to 25 September, 2004.

Figure 2.7. Spectra  $G(f)$  of noise recorded at the Odoptu-S-10 monitor station in good weather and during the build up to a storm.

Figure 3.1. Map of the study area showing the major facilities and pipeline routes as well as the AUAR deployment locations for the PTL experiments and the profiles surveyed.

Figure 3.2. (a) Velocity  $C(z,r)$  distribution along TL profile PTL11 and results of frequency dependent TL(f) experiments acquired in (b) Good weather and (c) Stormy weather.

Figure 3.3. PTL profile PTL1: (a) bathymetry and velocity  $C(z,r)$  along the profile as well as the source, receiver and intermediate hydrology locations. (b)



Frequency dependent TL plot showing the results for the source location.

- Figure 3.4. PTL profile PTL2: (a) bathymetry and velocity  $C(z,r)$  along the profile as well as the source, receiver and intermediate hydrology locations. (b) Frequency dependent TL plot showing the results for all the source locations (in different colors).
- Figure 3.5. PTL profile PTL3: (a) bathymetry and velocity  $C(z,r)$  along the profile as well as the source, receiver and intermediate hydrology locations. (b) Frequency dependent TL plot showing the results for all the source locations (in different colors).
- Figure 3.6. PTL profile PTL4: (a) bathymetry and velocity  $C(z,r)$  along the profile as well as the source, receiver and intermediate hydrology locations. (b) Frequency dependent TL plot showing the results for all the source locations (in different colors).
- Figure 3.7. PTL profile PTL5: (a) bathymetry and velocity  $C(z,r)$  along the profile as well as the source, receiver and intermediate hydrology locations. (b) Frequency dependent TL plot showing the results for all the source locations (in different colors).
- Figure 3.8. PTL profile PTL6: (a) bathymetry and velocity  $C(z,r)$  along the profile as well as the source, receiver and intermediate hydrology locations. (b) Frequency dependent TL plot showing the results for all the source locations (in different colors).
- Figure 3.9. PTL profile PTL7: (a) bathymetry and velocity  $C(z,r)$  along the profile as well as the source, receiver and intermediate hydrology locations. (b) Frequency dependent TL plot showing the results for all the source locations (in different colors).
- Figure 3.10. PTL profile PTL8: (a) bathymetry and velocity  $C(z,r)$  along the profile as well as the source, receiver and intermediate hydrology locations. (b) Frequency dependent TL plot showing the results for all the source locations (in different colors).
- Figure 3.11. PTL profile PTL9: (a) bathymetry and velocity  $C(z,r)$  along the profile as well as the source, receiver and intermediate hydrology locations. (b) Frequency dependent TL plot showing the results for all the source locations (in different colors).
- Figure 3.12. PTL profile PTL10: (a) bathymetry and velocity  $C(z,r)$  along the profile as well as the source, receiver and intermediate hydrology locations. (b) Frequency dependent TL plot showing the results for all the source locations (in different colors).
- Figure 3.13. PTL profile PTL11: (a) bathymetry and velocity  $C(z,r)$  along the profile as well as the source, receiver and intermediate hydrology locations. (b) Frequency dependent TL plot showing the results for all the source locations (in different colors).
- Figure 3.14. PTL profiles from locations PTL12-A and PTL13-A to the Orlan monitor station. (a) Schematic map showing the experimental layout (b) bathymetry and velocity  $C(z,r)$  along the profile from PTL12-A as well as

the source, receiver and intermediate hydrology locations. (c) Frequency dependent TL plot showing the results for both source locations.

**Figure 3.15.** PTL profiles from locations PTL12-A and PTL13-A to the Piltun-S monitor station. (a) Schematic map showing the experimental layout (b) Frequency dependent TL plot showing the results for both source locations.

**Figure 3.16.** TL profiles TLP-2 from the Orlan platform location to the Orlan and Arkutun-Dagi monitor station. (a) Schematic map showing the experimental layout (b) bathymetry and velocity  $C(z,r)$  along the profile as well as the source, receiver and intermediate hydrology locations.

**Figure 3.16.** TL profiles TLP-2 from the Orlan platform location to the Orlan and Arkutun-Dagi monitor station. (c) Frequency dependent TL plot showing the results for both receiver locations.

**Figure 3.17.** TL profiles TLP-6 from the Orlan platform location to the Piltun-S monitor station. (a) Schematic map showing the experimental layout (b) bathymetry and velocity  $C(z,r)$  along the profile as well as the source, receiver and intermediate hydrology locations.

**Figure 3.17.** TL profiles TLP-6 from the Orlan platform location to the Piltun-S monitor station and the A4 acoustic station. (c) Frequency dependent TL plot showing the results for both receiver locations.

**Figure 3.18.** Models of the acoustic waveguides used for the numerical modeling. Profiles from the PTL-12A, PTL13-A and Orlan locations to the Piltun-S monitor station.

**Figure 3.18.** Models of the acoustic waveguides used for the numerical modeling. Profiles from the PTL-12A, PTL13-A and Orlan locations to the Orlan monitor station.

**Figure 3.19.** Theoretical TL results estimated along the numerical model waveguides presented in Figure 3.18.

**Figure 3.20.** TL profile TLP-14 (a) Schematic map showing the experimental layout (b) bathymetry and velocity  $C(z,r)$  along the profile as well as the source, receiver and intermediate hydrology locations.

**Figure 3.20.** TL profile TLP-14 (c) Frequency dependent TL plot showing the results for both receiver locations (Odoptu-S-10 and Odoptu-S-20).

**Figure 4.1.** Sonogram  $G(f,t)$  and plot of the variation in sound pressure level with time  $D(\Delta f,t)$  for data recorded at the Piltun monitor station from 7 to 17 August, 2004.

**Figure 4.2.** Impulses recorded at the PA-B-20 monitor station on 19 September 2004.

**Figure 4.3.** Impulses recorded at the Orlan monitor station on 22 September 2004.

**Figure 4.4.** (a) Impulses of biogenic origin recorded at the PA-B-20 monitor station on 18 September 2004 (b) blow up of impulse Imp-1.

- Figure 4.5.** Impulses of biogenic origin recorded at the Arkutun-Dagi monitor station on 18 September 2004.
- Figure 4.6.** Acoustic pulses of unknown origin recorded at Arkutun-Dagi monitor station on 18 September 2004.
- Figure 5.1.** Ten-minute acoustic energy estimates for three frequency bands. The plot is for the PA-B-10 (7) Monitor station on 16 August 2004, when synchronous observations were being made at the South behavioral station.
- Figure 5.2.** Ten-minute acoustic energy estimates for three frequency bands. The plot is for the Odoptu-S-10 (10) Monitor station on 11 September 2004, when synchronous observations were being made at the 2nd behavioral station.
- Figure 5.3.** Ten-minute acoustic energy estimates for three frequency bands. The plot is for the Odoptu-S-10 (10) Monitor station on 19 September 2004, when synchronous observations were being made at the 2nd behavioral station.
- Figure 6.1.** The research vessel *Academik Oparin* from Top: ahead and Middle: astern Bottom: *Igor Maksimov*.
- Figure 6.2.** Acoustic characterization of the *Academik Oparin* using a hydrophone deployed from the stern of the *Igor Maksimov*. (a) Schematic of the experiment Spectrum  $G(f)$  showing the acoustic signature generated by the *Academik Oparin* as it sailed at (b) 12 knots 50 m from the hydrophone (c) 100 m from the hydrophone.
- Figure 6.3.** Acoustic signature of the *Academik Oparin* recorded by an AUAR at the Arkutun-Dagi monitor station. (a) Schematic showing the maneuvers of the *Academik Oparin* (b) Sonogram  $G(f,t)$  of data from the monitor station (c) Spectra  $G(f)$  showing the acoustic levels corresponding to the points on the schematic (a).
- Figure 6.4.** Acoustic signature of the *Academik Oparin* recorded by an AUAR at the Odoptu-S-10 monitor station. (a) Schematic showing the maneuvers of the *Academik Oparin* (b) Sonogram  $G(f,t)$  of data from the monitor station (c) Spectra  $G(f)$  showing the acoustic levels corresponding to the points on the schematic (a).
- Figure 6.5.** Acoustic signature of the *Academik Oparin* recorded by an AUAR at the Piltun-S monitor station. (a) Schematic showing the maneuvers of the *Academik Oparin* (b) Spectra  $G(f)$  showing the acoustic levels corresponding to the *Academik Oparin* drifting with its engine operational (13:26) and with its engine shut down (13:35).
- Figure 6.6.** (a) Schematic showing the experimental design. Results of acoustic measurements of the zodiac 40 hp outboard motors recorded at location 5 while the zodiac was sailing at 7 km/h from point 2 to point 1: (b) 4-stroke engine (c) 2-stroke engine.
- Figure 6.7.** Results of acoustic measurements of the zodiac 4-stroke 40 hp outboard motor recorded at location 5 (a) Sonogram  $G(f,t)$  (b) spectrum  $G(f)$  (c) Low frequency spectrum  $G(f)$ .

- Figure 6.8.** Results of acoustic measurements of the zodiac 2-stroke 40 hp outboard motor recorded at location 5 (a) Sonogram  $G(f,t)$  (b) spectrum  $G(f)$  (c) Low frequency spectrum  $G(f)$ .
- Figure 6.9.** (a) Spectra  $G(f)$  of acoustic measurements of the zodiac 4-stroke 40 hp outboard motor sailing at 7 km/h and 25 km/h recorded at the closest point of approach to location 5 by the (b) Low frequency part of spectrum.
- Figure 6.10.** (a) Spectra  $G(f)$  of the 2-stroke and 4-stroke 40 hp outboard motors for Zodiacs sailing at 25 km/h recorded at the closest point of approach to location 5 (b) identical plot for Zodiacs sailing at 7 km/h.
- Figure 7.1.** Map of the NE Sakhalin Shelf showing the bathymetric grid (a) and locations where vertical hydrologic profiles were acquired.
- Figures 7.2.** Bathymetric map of the study area with contours. Note the dominant NE-SW orientation of the bathymetric structures.
- Figure 7.3.** 3D bathymetric map of the study area.
- Figure 7.4.** Map of the study area showing the locations where vertical hydrologic profiles were acquired.
- Figure 7.5.** Simplified scheme of water circulation in the Sea of Okhotsk, the dotted line is the Eastern Sakhalin current. Based on current maps by Shrenk L.I. (1874), Leonov A.K. (1960) and Moroshkin K.V. [Гидрометеорология и гидрохимия морей, 1998].
- Figure 7.6.** Schematic showing the structure of the thermohaline front on the NE Sakhalin shelf. Top: temperature; Bottom: Salinity.
- Figure 7.7.** Schematic showing the proposed near shore water circulation in an area with an irregular bottom (after Leont'ev).
- Figure 7.8.** Vertical profiles of temperature (T) and salinity (S) averaged for (a) August and (b) September for three different locations with depths up to (left) 20 m; (middle) 30 m; and (right) 40 m.
- Figure 7.9.** (a) - Map showing the location of profile #2.
- Figure 7.9.** (b) - Temperature field  $T(z,r)$  for profile #2. (a) Low tide; (b) High tide.
- Figure 7.9.** (c) - Salinity field  $S(z,r)$  for profile #2. (a) Low tide; (b) High tide.
- Figure 9.1.** The variation in amphipod density (purple) and bivalve biomass (M) overlain on the bathymetry of the study area.

## Executive Summary

In 2004 the Pacific Oceanological Institute (POI) deployed 13 Autonomous Underwater Acoustic Recorders (AUARs) to conduct acoustic measurements on the NE Sakhalin shelf as part of the gray whale research program. The goal of the program was to measure key acoustic and hydrologic data, thus allowing an estimate of the noise propagation to the Korean-Okhotsk gray whale (*Eschrichtius robustus*)<sup>1</sup> feeding areas to be made.

The 2004 acoustic program measured anthropogenic and ambient noise levels, conducted bathymetric and hydrologic surveys and made Transmission Loss (TL) measurements along profiles from the proposed pipeline routes to the eastern and southern edges of the Piltun feeding area. These TL measurements will be used to calibrate acoustic models that, in conjunction with the recorded spectra of noise sources will be used to predict the level of noise received in the gray whale feeding areas. The model predictions of the acoustic footprint will be used to plan construction operations and will aid in determining the appropriate mitigation measures to be applied. These measurements showed that for profiles extending from deep water to shallow water, the bathymetry and velocity field significantly affects the received acoustic field. For long shallow profiles, such as those parallel to the coast, reflections from the bottom and sea surface have the greatest impact on acoustic propagation.

Ambient noise measurements were taken in weather conditions ranging from a cyclone to calm seas. These measurements correlated well with relationships between noise and sea-state described in the literature. The acoustic signatures of the *Academik Oparin* and the outboard motors on the Photo-ID zodiacs were analyzed. The 4-stroke outboard motor was found to be quieter than the 2-stroke motor across the entire frequency spectrum.

A comprehensive bathymetric and hydrologic program was conducted in 2004, consisting of 8400 km of bathymetry data and 323 vertical hydrologic profiles. This data was used to build a bathymetric map of the area and to study the spatial and temporal variation of hydro-physical parameters under the influence of tides and cyclones. The shelf zone was relatively mixed, whereas the deeper water was more clearly stratified.

---

<sup>1</sup> The Korean Okhotsk (western) gray whale population is listed as endangered in the Russian Red Book and critically endangered by the International Union for the Conservation of Nature (IUCN).

## 1 Introduction

The shallow water (6 - 15 m) part of the NE Sakhalin shelf starting south of the mouth of Piltun Bay and extending northwards up the Sakhalin coast is one of the most important summer feeding areas for the Korean-Okhotsk (western) gray whales. Mother-calf pairs have also been seen in water depths of less than 10 m in the Piltun feeding area. Acoustic studies have been conducted in the area since 1999 since some of the planned oil and gas developments are near the Piltun feeding area. In 2001, another gray whale feeding area was discovered offshore in deeper water (30-50 m) approximately 20 km to the South East of the mouth of Chayvo Bay<sup>2</sup>.

The acoustic program conducted on the NE shelf of Sakhalin Island in 2004 had four main objectives:

1. The first was to study both temporal and spatial variations in the amplitude and frequency characteristics of ambient and anthropogenic sound at a series of monitoring stations located throughout the development area. These monitoring stations were positioned to be at the nearest outside edge of a gray whale feeding area to a proposed facility. The goal of this annual acoustic monitoring program is to estimate and measure any increase in the cumulative acoustic level in the gray whale feeding areas due to the oil development and production activities.
2. The second objective was to study sound propagation and the variation in frequency dependent Transmission Loss (TL) from the proposed pipeline routes to the nearest gray whale feeding area. These include the pipelines from Moliqpaq and PA-B as well as from Orlan to Chayvo. These TL profiles would allow an estimation of the increase in acoustic levels that could be expected if a facility with a defined acoustic signature was installed at the proposed location.
3. The third objective was to acquire a comprehensive grid of bathymetric and hydrologic data across the study area, and to investigate the spatial and temporal variations in the hydrology due to weather events (e.g. typhoons).
4. The final objective was to measure the acoustic levels of the two outboard motors used for the Photo-ID zodiacs (one 2-stroke and one 4-stroke) as well as the *Academik Oparin* (under different operational scenarios).

---

<sup>2</sup> Gray whales were seen feeding in the Offshore feeding area throughout the 2002-2003 field seasons.

The report for the 2004 acoustic program has been divided into two separate volumes. Volume 1 describes the equipment used for the 2004 program, its testing and calibration as well as the operational strategy and methodology for the 2004 field program [Borisov et. al., 2005]. The first volume also includes a CD with sonograms for all the data displayed in 24-hour segments and plots of the bathymetry data recorded in 2004.

This report (Volume 2) is dedicated to analysis of the data, conclusions, and recommendations for future work. The analysis includes a quantitative spectral analysis of the variation in ambient acoustic level with weather conditions and TL analysis. The TL analyses were conducted from the proposed PA-B and Molikpaq pipeline routes to the Piltun feeding area and from the Chayvo pipeline route to the Piltun and Offshore feeding areas. The report also contains an analysis of the acoustic characteristics of the research vessel *Academik Oparin* and the 2-stroke and 4-stroke outboard motors on the Photo-ID zodiacs. Finally, bathymetric and hydrologic data acquired during the 2004 field season was used to construct a bathymetric map of the area and to evaluate the variation in hydrologic parameters (temperature and salinity) with tidal and weather conditions.

### **1.1 Acoustic recording and processing equipment**

In 2004, POI FEB RAS<sup>3</sup> (POI) used the five AUARs designed and constructed in 2003, and eight newly fabricated AUARs<sup>4</sup>. These individually deployed AUARs were used to make acoustic measurements in the frequency band from 1 Hz to 15 kHz (Figure 1.1).

The AUARs<sup>5</sup> are made of welded titanium alloy and are rated to depths of up to 100 m. Two external sensors (hydrophones, accelerometers or hydrologic measuring equipment) can be input to the AUAR electronics. Inside the AUAR there are batteries secured in a titanium frame and a tray containing the AUAR electronics and power handling circuitry. The number of batteries depends on the AUAR design. The 2003 AUARs have two sealed batteries which can provide continuous operation of the AUAR for over 18 days, and the 2004 AUARs have three sealed batteries providing continuous operation of the AUAR for

---

<sup>3</sup> POI FEB RAS - The Pacific Oceanological Institute, Far East Branch of the Russian Academy of Sciences.

<sup>4</sup> The eight new AUARs were designed to improve the operational handling of the units following the experiences of the 2003 field program.

<sup>5</sup> 2003 AUAR dimensions are length 0.8 m, diameter 0.38 m, weight in air ~105 kg. 2004 AUAR dimensions are length 1.2 m, diameter 0.32 m, weight in air ~105 kg.

over 15 days.<sup>6</sup> Cylindrical hydrophones (model # GI-50 (ГИ-50)) and Spherical hydrophones of type G61H (Г61H) both with integrated pre-amplifiers designed specifically for the hydrophones were used for the AUARs.



**Figure 1.1 - 2003 and 2004 AUARs being prepared for deployment.**

The AUARs digital recorder is based on the Prometheus single board computer, which has an integrated 16 bit analog to digital converter (ADC). In order to optimize the dynamic range of the 16 bit ADC, the signal amplitudes should be equal across the entire frequency range. However, ambient noise generally has an amplitude maximum at low frequencies and drops off with higher frequencies. The ADC does not have the dynamic range to record frequencies from 1 Hz to 15 kHz. The AUAR therefore has two analog channels: a Low Frequency (LF) channel with no correction and a High Frequency (HF) channel with the low

---

<sup>6</sup> The two sealed batteries (2003) have a capacity of 115 Ampere-hours. The three sealed batteries (2004) have a capacity of 115 Ampere-hours.



frequency component (<1.5 kHz) removed by a low cut filter. This allows the gain coefficient for frequencies above 1 kHz to be increased without overloading the ADC.

The primary AUAR data storage is a compact laptop 80 GB hard drive. To prevent electromagnetic and acoustic noise generated by the rotating hard drive from contaminating the data a 489 MB or 1 GB flash memory drive is used as a buffer. While data is being recorded on the flash drive the hard drive is in standby mode with its motor off. When the flash memory drive is full, the recording cycle is halted while the flash memory drive writes to the hard drive; the data therefore contains controlled gaps. The size of these gaps depends on the size of the flash memory drive and the recording parameters<sup>7</sup>.

A floating buoy connected to a 24 kg anchor by a 70 m rope marks the location of the AUAR on deployment. This anchor is linked to the AUAR by a 150 m long rope weighted down with lead weights. If necessary the vessel can grapple for the 150 m rope between the anchor and the AUAR since the GPS coordinates of both are logged during deployment. The AUAR can therefore still be recovered in the event that the surface buoy is lost; one AUAR was recovered in this manner during the 2003 field season.

Practical experience has shown that at shallow deployment depths (10-30 m), movement of the surface buoy due to wave action can be mechanically conducted down the rope to the hydrophone, where this mechanical movement can be recorded as acoustic noise. The AUAR is deployed so as to reduce this noise by isolating the hydrophone from the surface buoy with an anchor, thus reducing the mechanical coupling between the surface buoy and the hydrophone. The hydrophone is also deployed 15 m from the AUAR to prevent distortion of the acoustic field by scattering or masking by the AUAR container at high frequencies. The hydrophone is deployed inside a pyramid shaped wire frame and attached by rubber bands to the frame, isolating it to the best extent possible from the sea floor.

In 2004 the *Academik Oparin* was the operational platform for the entire acoustic program, as well as the vessel-based biology programs (Photo ID, Benthic, Marine Mammal Observers (MMO)).

---

<sup>7</sup> For a 489 MB flash memory drive the gap was approximately 9 minutes every 3.5 hours, and for a 1 GB flash drive it was approximately 24 minutes every 7 hours (LF channel).

During the 2004 field season AUARs were deployed and synchronous acoustic measurements recorded at stations ranging from near the Odoptu well pads to the center of the Offshore feeding area (Figure 1.2 and Table 1.1), an area that extended 100 km up the NE Sakhalin shelf. Before each AUAR is deployed, its computer is programmed for the desired recording schedule. Computers on the *Academik Oparin* were used as the main data storage units. The acoustic data on the AUAR hard drive was copied to CD's and a removable hard drive before the files on the AUAR drive were deleted prior to redeployment.

To compute TL from acoustic measurements made by different AUARs, the data has to be calibrated to an absolute pressure standard. The hydrophones were manufactured with nominal sensitivities and the gains were set in the field. Field cross-calibrations conducted in 2004 confirmed the absolute calibration of the data. Further details of the AUARs used, their location, deployment depth and recording settings can be found in Appendix A. A detailed description of the characteristics and calibration of the 2004 acoustic recording equipment is provided elsewhere [Borisov et. al., 2005].

## **1.2 Low Frequency and High Frequency transducers and hydrological sonde**

A low frequency (LF) resonant electromagnetic transducer and high frequency (HF) piezoelectric broadband transducer deployed from the *Academik Oparin* were used for sound propagation and TL studies at frequencies from 15-15000 Hz. The acoustic level of signals generated by the transducers was monitored using a calibrated hydrophone and recorded on the *Academik Oparin*<sup>8</sup>. The LF transducer has a cylindrical container filled with gas<sup>9</sup>, and a pair of identical closely spaced radiating pistons oscillating in opposite directions creating a volume displacement<sup>10</sup>. An electromagnetic controller controls the motion of the pistons; hydrostatic compensation is achieved using an air pump. The LF resonance transducer was deployed at a depth of 8 m from the anchored *Academik Oparin*. The 27 Hz acoustic signal has an intensity of ~180 dB re 1  $\mu\text{Pa}^2/\text{Hz}$  at 2 m from the transducer. The HF broadband piezoelectric (ceramic) transducer is cylindrical<sup>11</sup> and consists of seven

---

<sup>8</sup> While the transducers were operating the acoustic signal levels were measured using a calibrated hydrophone located 1 - 2 m away from the transducer.

<sup>9</sup> Dimensions are diameter 58 cm, height 15 cm, weight 48 kg in air, ~6 kg in water.

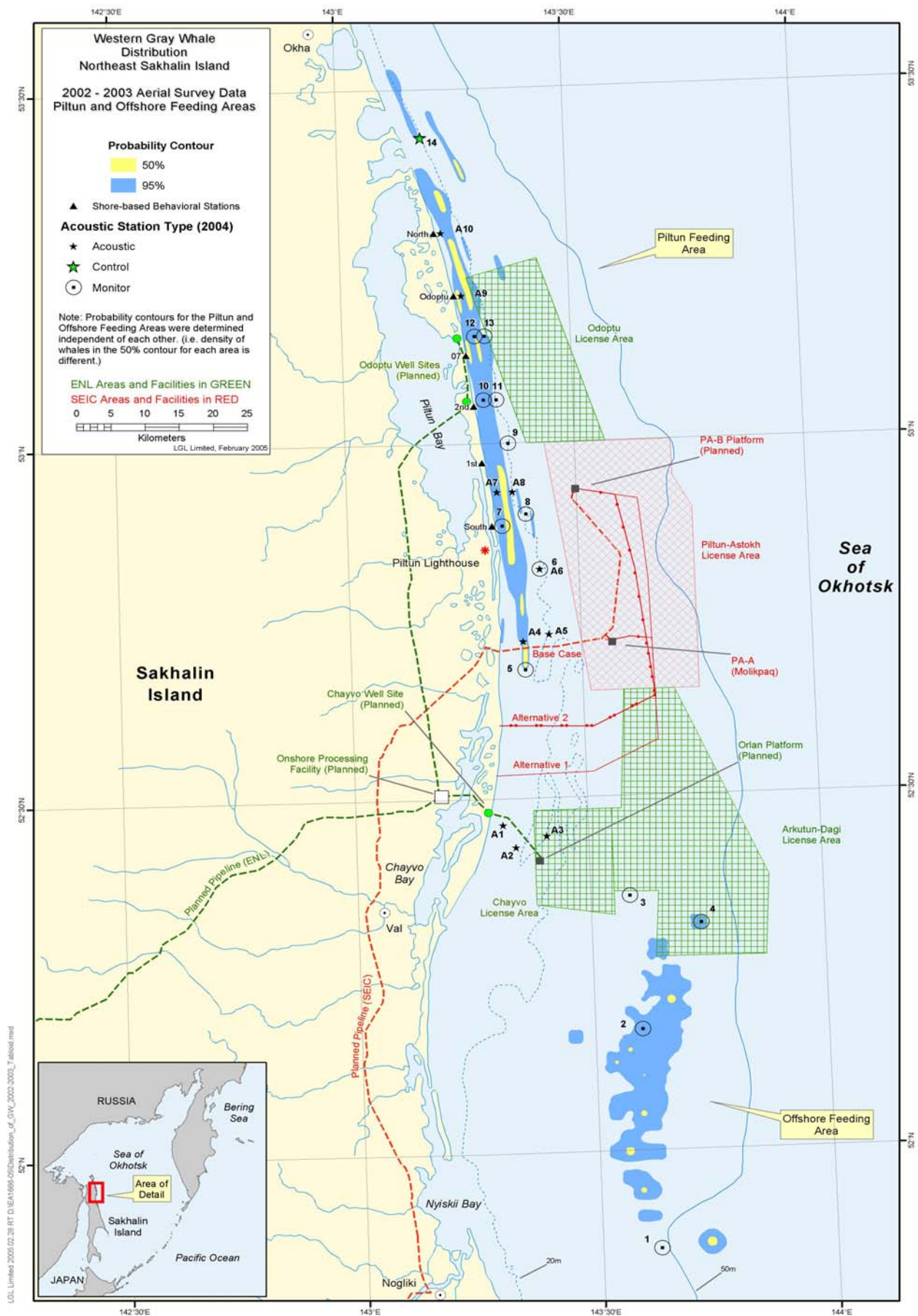
<sup>10</sup> Tests in the Sea of Japan using calibrated accelerometers, and conducted at a depth of 2 m, indicated that when the maximum number of springs (30) are used, the resonance frequency of the transducer is 20.2 Hz with marginal frequencies of 15.2 and 30.6 Hz (-3 dB).

<sup>11</sup> Dimensions are diameter 28 cm, height 136 cm, weight ~ 60 kg in air, ~ 15 kg in water.

piezoelectric rings connected in parallel coated with a composite material and sealed at the ends with a metal shield.

**Table 1.1 - Numbers, names, locations and depths of the proposed stations.**

#	Station		Latitude	Longitude	Depth
Monitor Stations:					
1	Lunskoye	Лунское	51° 51' 45" N	143° 37' 27.3" E	50 m
2	OFA (Offshore Feeding area)	ГЗК (Глубоководная зона кормления)	52° 10' 18" N	143° 36' 1.8" E	~40 m
3	Orlan	Орлан	52° 21.6' N	143° 35.0' E	32 m
4	Arkutun-Dagi	Аркутун-Даги	52° 19' 9.6" N	143° 44' 4.6" E	~40 m
5	Piltun-S	Пильтун-Ю	52° 40' 51" N	143° 22' 34" E	10 m
6	Piltun	Пильтун	52° 49.3' N	143° 24.9' E	20 m
7	PA-B-10	ПА-Б-10	52° 53' 2.1" N	143° 20' 10.6" E	10 m
8	PA-B-20	ПА-Б-20	52° 54' 00" N	143° 23' 20.5" E	20 m
9	Odoptu-PA-B	Одопту-ПА-Б	53° 00' 00" N	143° 21' 18" E	20 m
10	Odoptu-S-10	Одопту-Ю-10	53° 03.7' N	143° 18.3' E	10 m
11	Odoptu-S-20	Одопту-Ю-20	53° 03' 42" N	143° 19' 58" E	20 m
12	Odoptu-N-10	Одопту-С-10	53° 09.1' N	143° 17.4' E	10.5 m
13	Odoptu-N-20	Одопту-С-20	53° 09' 6" N	143° 18' 42" E	20 m
14	Control	Контрольная	53° 25.95' N	143° 11.1' E	20 m
Acoustic Stations:					
A1	#1 (Chayvo-1)	#1 (Чайво-1)	52° 27.8' N	143° 19.0' E	11 m
A2	#2 (Chayvo-2)	#2 (Чайво-2)	52° 25.9' N	143° 20.6' E	11 m
A3	#3 (Chayvo-3)	#3 (Чайво-3)	52° 26.8' N	143° 24.6' E	17 m
A4	#4 (Piltun-1)	#4 (Пильтун-1)	52° 43' 14.4" N	143° 22' 26.7" E	10 m
A5	#5 (Piltun-2)	#5 (Пильтун-2)	52° 43' 48" N	143° 25' 49" E	20 m
A6	#6 (Piltun-3)	#6 (Пильтун-3)	52° 49.3' N	143° 24.9' E	20 m
A7	#7 (PA-B-1)	#7 (ПА-Б-1)	52° 55' 54" N	143° 19' 39" E	10 m
A8	#8 (PA-B-2)	#8 (ПА-Б-2)	52° 55' 54" N	143° 21' 42.4" E	20 m
A9	#9 (BEH-Odoptu)	#9 (Одопту (Пов))	53° 12' 33.1" N	143° 15' 51" E	10 m
A10	#10 (BEH-north)	#10 (Пов-север)	53° 17' 52.4" N	143° 13' 25.4" E	10 m



In order to more accurately characterize the 2004 TL measurements, the hydrological characteristics (velocity, temperature, salinity and pressure) of the water layer were acquired using a hydrological sonde. The sonde is powered by a set of D cells, providing approximately 180 hours of continuous operation. 8400 km of bathymetric data and 323 vertical hydrologic profiles were acquired in 2004.

### 1.3 Terminology and algorithms used in the report

Ambient and anthropogenic noise recorded by the AUARs was written to disc in microPascals ( $\mu\text{Pa}$ )<sup>12</sup>. Acoustic spectra in decibels will be used to describe the variation in acoustic power as a function of frequency. In this report sound pressure power density spectra  $G(f)$  ( $\mu\text{Pa}^2/\text{Hz}$ )<sup>13</sup> will be used when spectral data are plotted. These spectra are often averaged over 10-300 one-second windows to improve the statistical stability of the ambient noise data<sup>14</sup>. The sonograms  $G(f,t)$  are plots of power spectral density vs. frequency and time, the scales generally run from ~37 to ~120 dB re 1  $\mu\text{Pa}^2/\text{Hz}$ . A detailed description of the methodology used for normalizing and calculating both the amplitude and spectral data is given in Borisov et.al. [2005], Appendix D.

### 1.4 Units

During the course of this report a number of different unit notations have been used. This is due to differences in standard notation between different disciplines and nationalities. The following are equivalent units using the different standard nomenclatures:

1 mkPa = 1  $\mu\text{Pa}$  and 1 mkV = 1  $\mu\text{V}$ .

For spectral density plots: Although the units for power spectral density are  $\mu\text{Pa}^2/(\text{s Hz})$ ,  $\mu\text{Pa}^2/\text{s/Hz}$  or  $\mu\text{Pa}^2$ , it is common usage to define the units for power spectral density as  $\mu\text{Pa}^2/\text{Hz}$  or  $\mu\text{Pa}/\sqrt{\text{Hz}}$ .

---

<sup>12</sup> The data was scaled (after incorporating hydrophone sensitivity and system gain) to convert the data to standard units of pressure (measured through an omni-directional hydrophone) in real time.

<sup>13</sup> Energy and power spectra are scaled to 1 Hz whatever the analysis length.

<sup>14</sup> Average of 10 or 300 1-second spectral realizations; the analysis window length is shown on the plot. Spectral averaging will lead to a lower variance spectral estimate.

## 2 Impact of weather conditions on the ambient acoustic field of the NE Sakhalin shelf

This section analyzes the ambient noise measurements recorded in 2004 and discusses the variation in ambient noise with meteorological conditions and Sea State. The acoustic measurements are analyzed in both the frequency and time domain.

Previous reports have discussed the variation in ambient noise due to wind, surface waves and rain. For example, the broadband noise level near Chayvo rose by 12 dB when the sea state increased from 1 to 4 [Borisov et.al., 2003]. A rainstorm with strong wind squalls pushed the ambient noise level 16-18 dB higher. For frequencies above 2.5 kHz, the spectral level of ambient noise recorded during a storm reached ~64 dB re 1  $\mu\text{Pa}^2/\text{Hz}$  (56 dB re 1  $\mu\text{Pa}^2/\text{Hz}$  for a storm without rain). In 2003, the acoustic measurements were conducted using AUARs. Spectral analysis of the data acquired in 2003 showed that the noise field in the frequency band from 200-800 Hz generated by an approaching storm had the clear interference structure resulting from waveguide propagation on the shelf [Borisov et.al., 2004]. The data showed that noise produced by wind and surface waves is much lower for shallow water (10 m) than for areas outside the 20 m contour. The highest ambient noise level was recorded in the frequency band from 200-1000 Hz. The ambient noise in this frequency band reached 71 dB re 1  $\mu\text{Pa}^2/\text{Hz}$  during a storm and 46 dB re 1  $\mu\text{Pa}^2/\text{Hz}$  in calm weather.

In 2004 as in 2003, the acoustic data was recorded using AUARs and ambient noise data was acquired at monitoring stations across the area. This allowed the variation in ambient noise level with location and weather conditions to be studied. The AUAR at location A.5 (Figure 1.2) recorded data continuously during the period when a powerful typhoon was crossing the shelf. Figure 2.1 shows a sonogram  $G(f,t)$  and a plot of the variation in sound pressure level with time and frequency band  $D(\Delta f, t)$ <sup>15</sup>.

$$D(\Delta f, t) = 10 \log \int_{f_1}^{f_2} \hat{G}(f, t) df \quad \Delta f = f_1 - f_2 \quad (2.1)$$

---

<sup>15</sup> The four frequency bands used for estimating sound pressure level for Figure 2.1 and all other figures are 20-800 Hz, 800-2000 Hz, 2000-10000 Hz and 20-10000 Hz. This measure quantifies the acoustic level within the specified frequency band.



# Point-A5, 28.08-8.09.2004

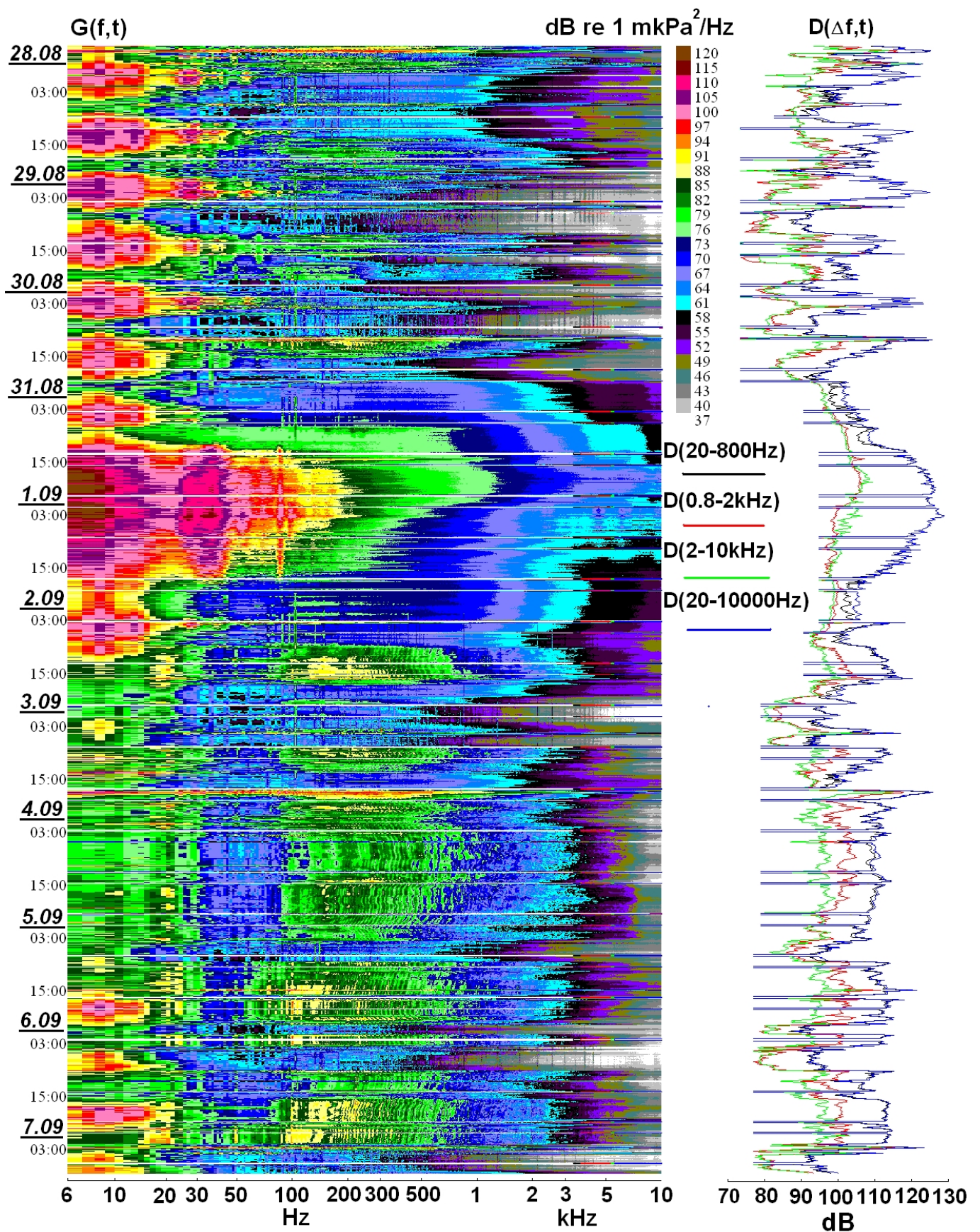


Figure 2.1 - Sonogram  $G(f,t)$  and plot of the variation in sound pressure level with time  $D(\Delta f, t)$  over four frequency ranges for data recorded at location A.5 during a typhoon.

Figure 2.1 shows that twice a day tidal currents cause intense flow noise at frequencies below 20 Hz. Rotational water movement in surface waves during the typhoon could lead to even higher flow noise and may even move the hydrophone deployed at 20 m (Figure 2.1: sonogram  $G(f,t)$  - 31 August to 1 September). This mechanical motion caused clipping in some of the data. Non-clipped data in the frequency range from 5-15000 Hz was therefore analyzed for data recorded at location A.5.

The ambient noise level at acoustic station A.5, located at the SE border of the Piltun feeding area (20 m depth) can be compared with the level at the Arkutun-Dagi monitor station (42 m depth) positioned at the northern border of the Offshore feeding area. Figure 2.2 displays synchronous and close to synchronous<sup>16</sup> spectra  $G(f)$  of data recorded at acoustic station A.5 (Figure 2.2(a)) and the Arkutun-Dagi monitor station (Figure 2.2(b)). The spectral density plot  $G(f)$  for 6:53 (Figure 2.2: 31.08 - 6:53) corresponds to good weather conditions, however the vessel *Trias* was close to acoustic station A.5. The Broadband sound level above 7 kHz has dropped below the internal noise level of the AUAR (~35 dB re 1  $\mu\text{Pa}^2/\text{Hz}$ ). As the typhoon approached, most vessels sailed to the NE to find shelter from the storm. The spectral density plots  $G(f)$  for 17:48, 03:34, and 13:10 illustrate the increase in the acoustic levels due to wind and surface waves. Figure 2.2 shows that the broadband spectral levels increased by more than 20 dB (for the frequency band from 100-15000 Hz) in a heavy storm (Figure 2.2: 03.34 and 13.10 relative to 06.53). The plot for 13.10 even exceeds the predicted spectral levels for Sea State 6 (SS-6: wind - 17.5-20.6 m/s, waves - 4-6 m) [Knudsen et. al., 1948; Richardson et. al., 1995].

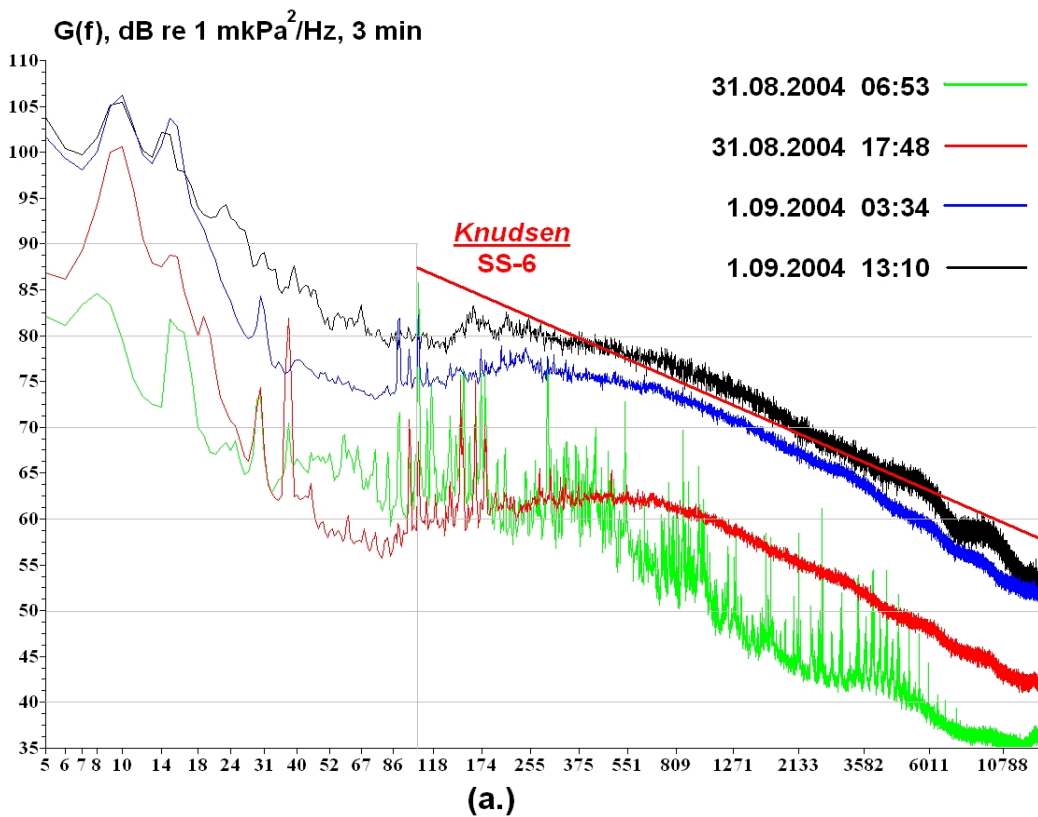
The spectra from Figure 2.2 (Figure 2.2(a): 1.09-03:34 and Figure 2.2(b) 1.09-02.40) show that in the frequency band between 0.1-10 kHz the spectral levels of storm generated noise at acoustic station A.5 and the Arkutun-Dagi monitor station (50 km apart) are similar. The spectra for 17:48 on 31 August are different because they correspond to different phases of the storm. The storm was generated by a cyclone moving to the north.

---

<sup>16</sup> The AUAR at the Arkutun-Dagi monitor station switched off at 2.50 on 1 September 2004.



Point-A5, 31.08-1.09.2004



Point-4 - Arkutun-Dagi, 31.08-1.09.2004

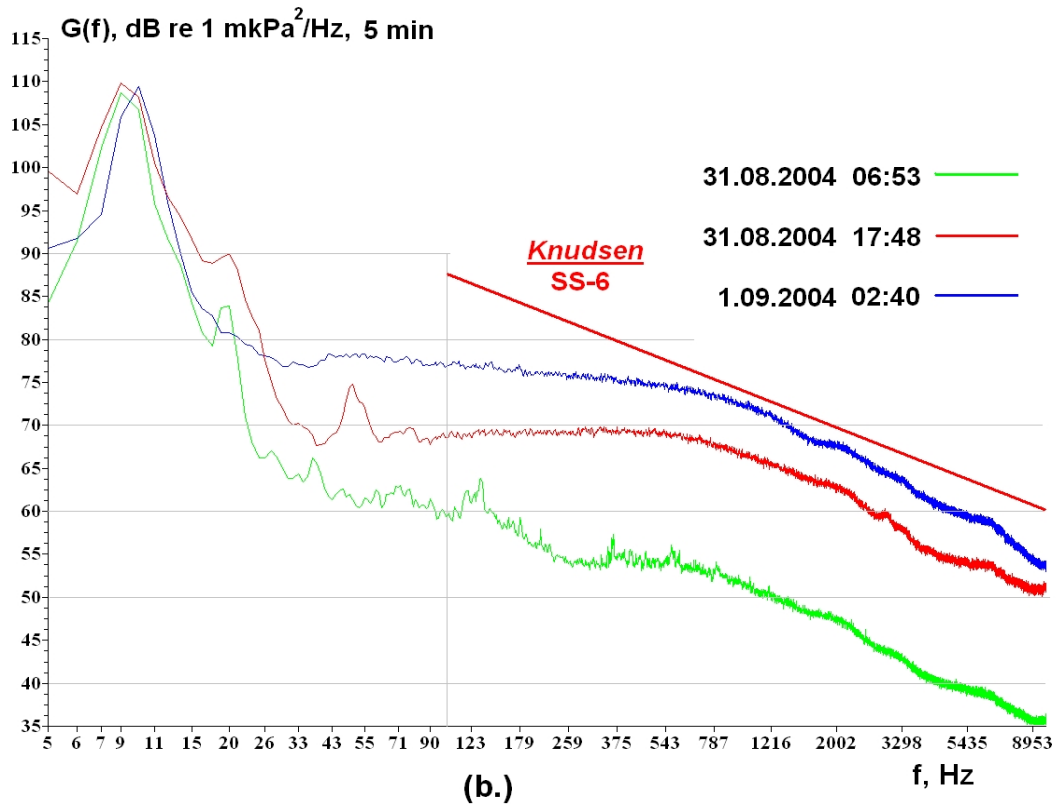


Figure 2.2 - Spectra  $G(f)$  of noise synchronously (or close to synchronously) recorded at (a) acoustic station A.5 and (b) monitor station Arkutun-Dagi during a typhoon.

Figure 2.3 shows a sonogram  $G(f,t)$  for the data recorded at the Arkutun-Dagi monitor station from 19 to 31 August. This data shows that this area was also affected by a heavy storm on 25 August. Figure 2.4 gives a sonogram  $G(f,t)$  and spectra  $G(f)$  for different phases of the storm and compares the spectral density levels to those recorded at the Arkutun-Dagi monitor station in good weather.

The sonogram  $G(f,t)$  (Figure 2.4(a)) shows a distinct interference structure between 10:00 and 11:00 on 24 August, the low frequency tonal components are very clear, this is probably caused by a distant passing vessel. The sonogram  $G(f,t)$  (Figure 2.4(a)) shows a relatively smooth increase in ambient noise level as the storm develops. The spectra  $G(f)$  demonstrate that the transition from a relatively calm sea state (Figure 2.4(b): 23.08-22:30) into a stormy sea state (Figure 2.4(b): 24.08-05:00) led to a sharp increase of noise (almost 20 dB) in the frequency band from 300-10000 Hz. At this point the spectral shape stabilized, but the overall spectral level did not increase significantly. These spectra (Figure 2.4(b): 24.08-14:00 and 25.08-05:00) illustrate that a storm can generate broadband noise in the frequency range from 400-1000 Hz that is very similar to white noise, with spectral levels reaching 80 dB re 1  $\mu\text{Pa}^2/\text{Hz}$  in the Offshore feeding area. The spectrum  $G(f)$  for 26 August (Figure 2.4(b): 26.08-20:00) shows the spectrum for calm weather. The spectrum  $G(f)$  for 10:00 on 23 August shows the noise produced by the vessel *Academik Oparin* as it passed 5 Km from the Arkutun-Dagi monitor station. The broadband and tonal components below 1 kHz exceed the spectral levels recorded during a typhoon.

Figure 2.5 displays a spectral analysis of data recorded at the Arkutun-Dagi monitor station from 7 to 19 September 2004. The sonogram  $G(f,t)$  illustrates that there were two strong storms (9 and 17 September) during this time period. The sound pressure level  $D(\Delta f,t)$  plots quantify the acoustic level within the specified frequency bands. The acoustic signature of moving vessels is a set of narrow tonal components with most of the acoustic energy in the frequency band from 20-800 Hz<sup>17</sup>. The acoustic signature of weather events is a smoothly varying change in the ambient acoustic level with its acoustic energy spread across the spectrum from 20-15000 Hz<sup>18</sup>.

---

<sup>17</sup> There is little difference in the sound pressure level  $D(\Delta f,t)$  estimated from 20-800 Hz or 20-15000 Hz.

<sup>18</sup> The sound pressure level  $D(\Delta f,t)$  estimated from 20-800 Hz is significantly lower than from 20-15000 Hz.

# Point-4 - Arkutun-Dagi, 19-31.08.2004

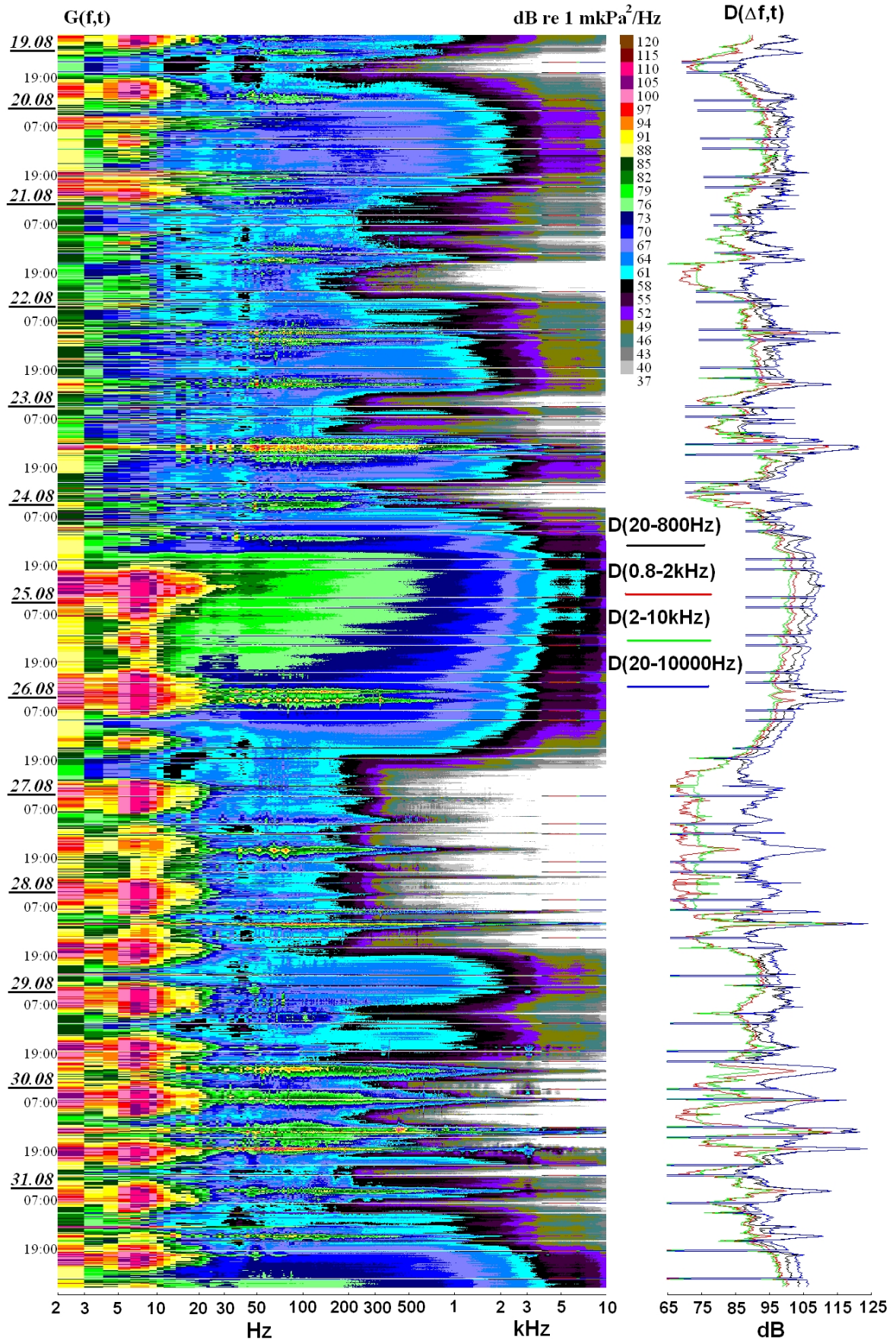
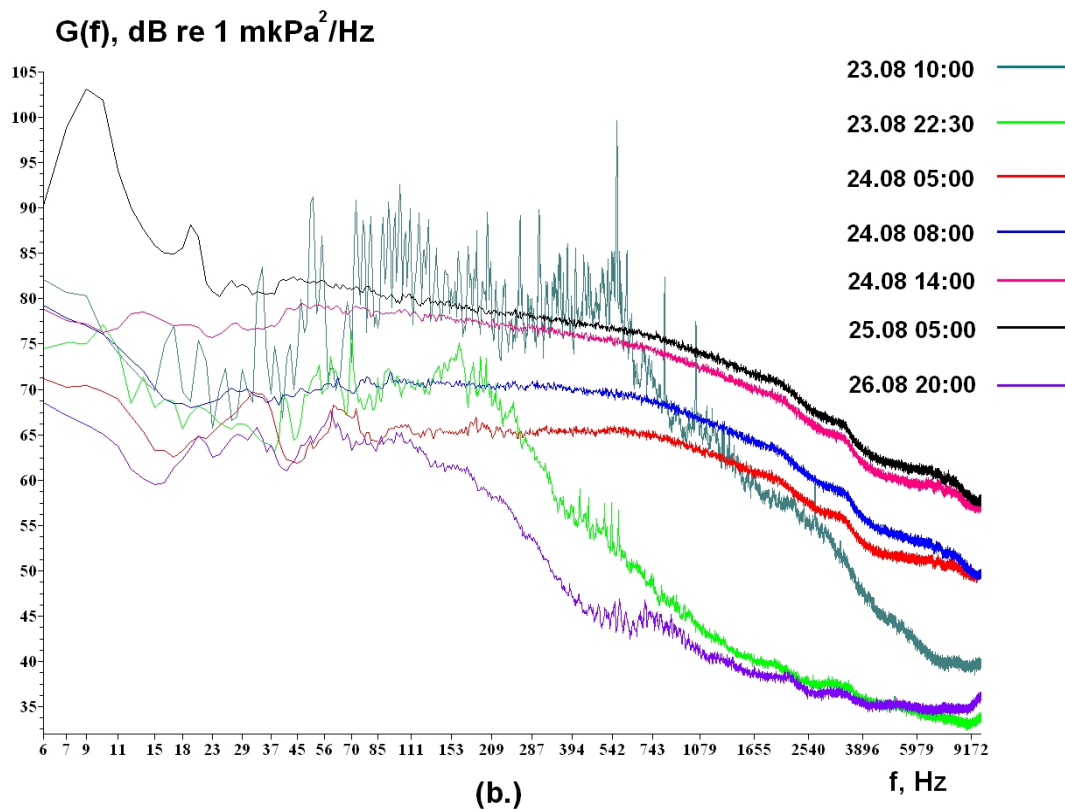
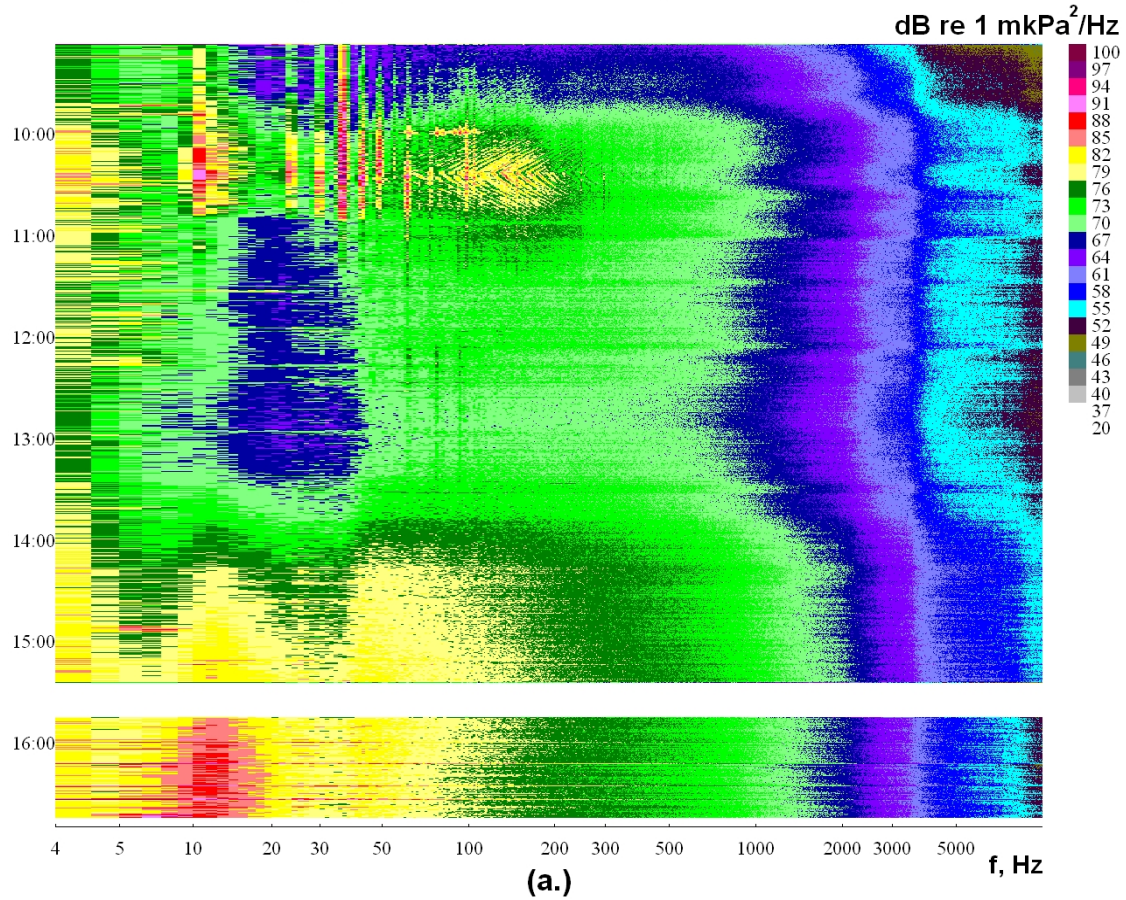


Figure 2.3 - Sonogram  $G(f,t)$  and plot of the variation in sound pressure level with time  $D(\Delta f, t)$  for data recorded at monitor station Arkutun-Dagi from 19 to 31 August, 2004.



**G(f,t), Point-4 - Arkutun-Dagi, 24.08.2004**



**Figure 2.4 - (a) Sonogram  $G(f,t)$  showing development of a storm on 24 August;  
(b) spectra  $G(f)$  of acoustic noise recorded at different phases of the storm -  
Arkutun-Dagi monitor station.**

# Point-4 - Arkutun-Dagi, 7-19.09.2004

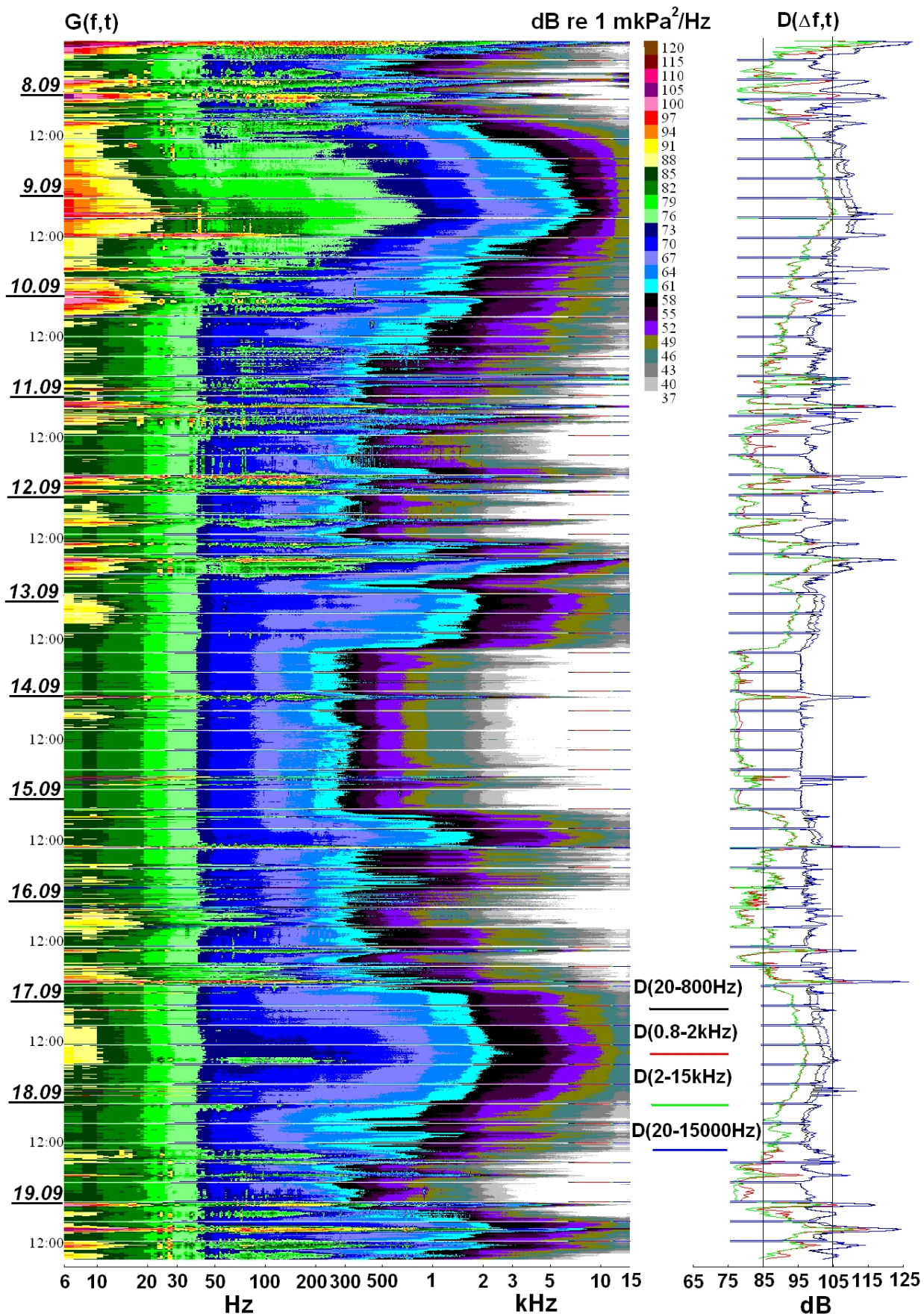


Figure 2.5 - Sonogram  $G(f,t)$  and plot of the variation in sound pressure level with time  $D(\Delta f,t)$  for data recorded at monitor station Arkutun-Dagi from 7 to 19 September 2004



Figure 2.6 shows the spectral analysis of data recorded at the Odoptu-S-10 monitor station from 10 to 25 September 2004<sup>19</sup>. Figure 2.6 shows that a storm moved in on the evening of 16 September and dissipated the morning of 18 September. The sonogram  $G(f,t)$  also shows the noise generated by the *Academik Oparin* as it maneuvered close by with transducers deployed from the vessel for the TL experiments (TLP-14) conducted on 10 and 12 September. Additionally, the *Academik Oparin* maneuvered in the area supporting Photo-ID, benthic and behavioral monitoring activity.

Figure 2.7 shows spectra  $G(f)$  corresponding to the different phases of the storm. The spectrum for 5:30 (Figure 2.7: 16.09-05:30) was recorded during good weather, the other spectra were recorded as the weather deteriorated. Figures 2.2, 2.4(b) and 2.7 display spectra  $G(f)$  showing different phases of storms. The spectra are similar except for Figure 2.7 where the depth at the monitor station was shallower (10 m). These shallow spectra show a minimum in the ambient noise level at low frequencies (e.g. Figure 2.7: 16.09-22:42). As the storm develops this minimum began to fill up, however it can still be seen in Figure 2.7: 17.09-20:30). In Figure 2.4(b) the spectra  $G(f)$  estimated from data recorded at a depth of 44 m during a storm do not show such a minimum.

---

<sup>19</sup> The Odoptu-S-10 monitor station is located at the 10 m contour offshore from the 2nd behavioral station.

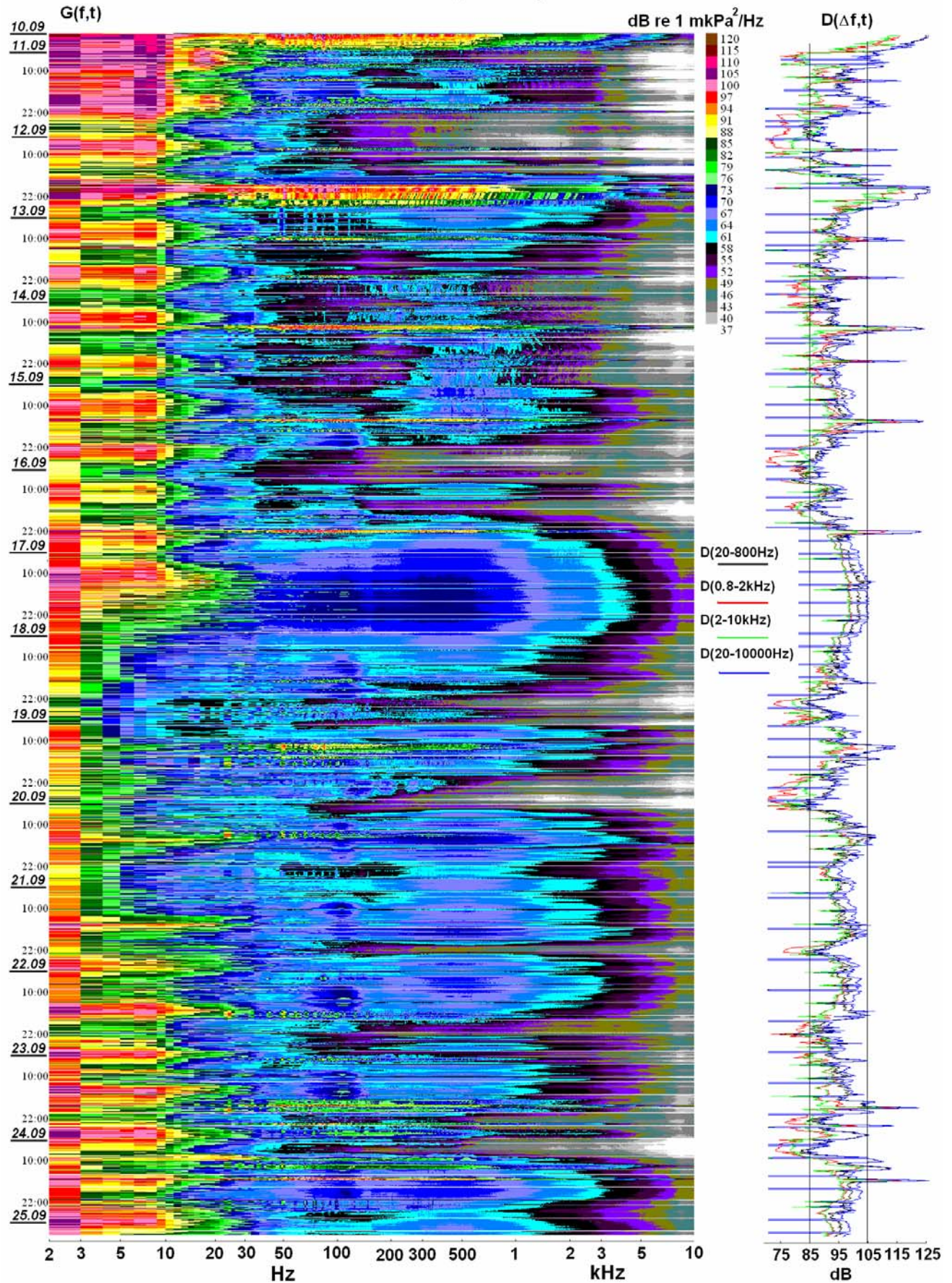


Figure 2.6 - Sonogram  $G(f,t)$  and plot of the variation in sound pressure level with time  $D(\Delta f,t)$  for data recorded at monitor station Odoptu-S-10 from 10 to 25 September, 2004.

Point-10 - Odoptu-S-10, 16-17.09.2004

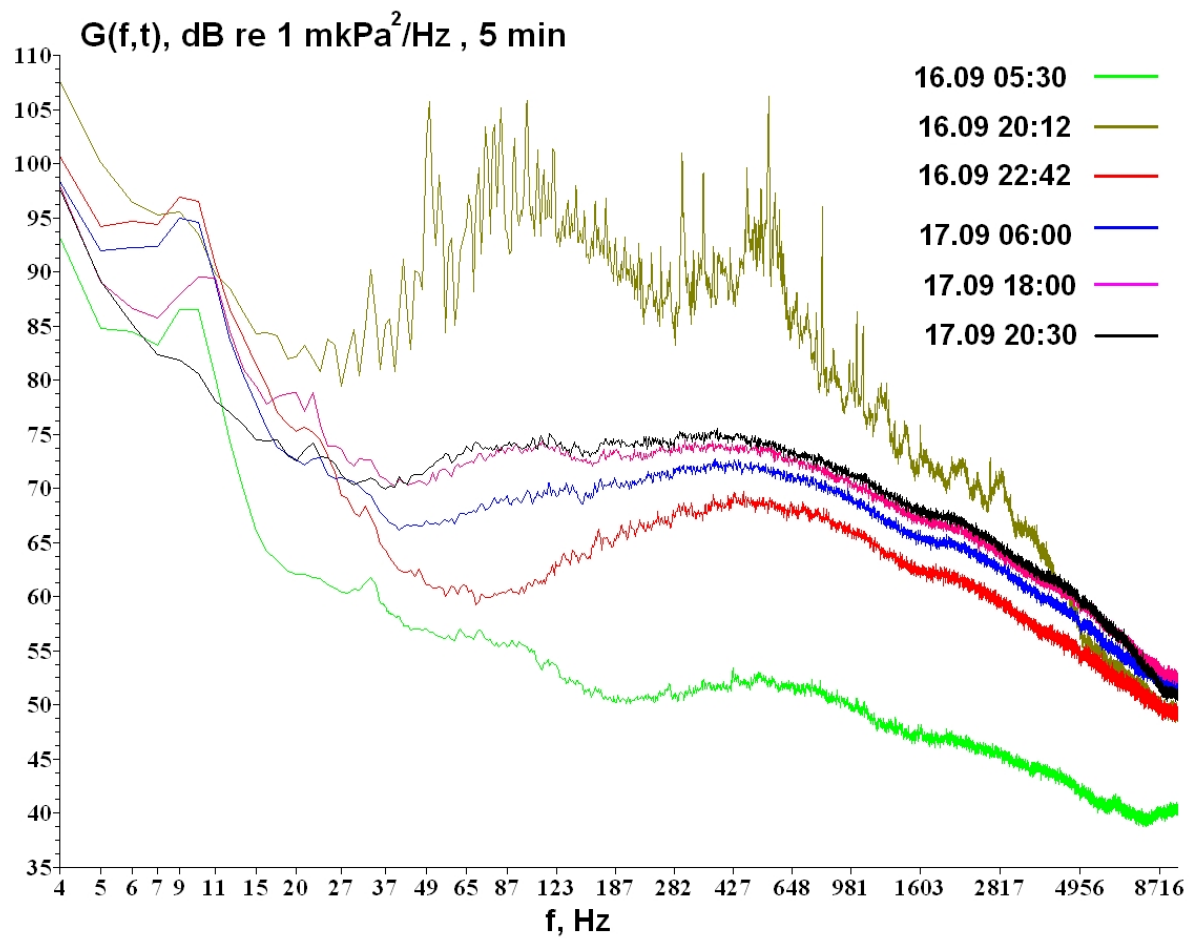


Figure 2.7 - Spectra  $G(f)$  of noise recorded at the Odoptu-S-10 monitor station in good weather and during the build up to a storm.